Polarization dependence of radial breathing mode peaks in resonant Raman spectra of vertically aligned single-walled carbon nanotubes

Zhengyi Zhang,[1,2] Erik Einarsson,[1] Yoichi Murakami,[3] Yuhei Miyauchi,[4,5] and Shigeo Maruyama[1,*]
[1]*Department of Mechanical Engineering, The University of Tokyo, 7-3-1 Hongo, Bunkyo-ku, Tokyo 113-8656, Japan*
[2]*Department of Mechanical Engineering, Columbia University, New York, New York 10027, USA*
[3]*Global Edge Institute, Tokyo Institute of Technology, 2-12-1 Ookayama, Meguro-ku, Tokyo 152-8550, Japan*
[4]*Institute for Chemical Research, Kyoto University, Uji, Kyoto 611-0011, Japan*
[5]*Center for Integrated Science and Engineering, Columbia University, New York, New York 10027, USA*
(Received 24 September 2009; revised manuscript received 15 February 2010; published 29 April 2010)

Polarization-dependent resonance Raman spectra of a vertically aligned single-walled carbon nanotube (SWNT) array were measured such that the polarization of the scattered light was selected either parallel or perpendicular to that of the incident light. For the parallel configuration, radial breathing mode (RBM) peaks exhibited two different polarization angle dependencies. One group (dominated by a peak at 203 cm^{-1}) had a maximum scattering intensity for incident light parallel to the alignment direction whereas the other group (dominated by a peak at 181 cm^{-1}) had maximum intensity for excitation perpendicular to the alignment direction. This anomalous behavior has been attributed to resonance with nonvertical transitions due to perpendicularly polarized excitation [Y. Murakami *et al.*, Phys. Rev. B **71**, 085403 (2005)]. Here we systematically measure the polarization-dependent Raman spectra and compare to theoretical expectations for the two different configurations. The 203 cm^{-1} group peaks are found to behave as expected for parallel-polarized dipole excitation, however the 181 cm^{-1} group peaks deviate significantly from the prediction assuming perpendicularly polarized excitation. The 181 cm^{-1} group peak intensities were found to be both environment and morphology dependent, indicative of isolated SWNTs. Therefore, the sound interpretation of these results is that the apparently anomalous polarization dependence is not due to perpendicular RBM excitation but rather the parallel excitation of isolated SWNTs suspended within the array.

DOI: 10.1103/PhysRevB.81.165442 PACS number(s): 61.48.De

I. INTRODUCTION

There has been great interest in the optical properties of single-walled carbon nanotubes (SWNTs) due to their quasi-one-dimensionality. Divergences in the electronic density of states, so-called Van Hove singularities, give rise to the dominant $E_{\mu,\mu}$ intersubband transitions (where μ denotes the cutting line index[1]) for incident light polarized along the nanotube axis. However, cross-polarized absorption by SWNTs—which is possible by nonvertical ($E_{\mu,\mu\pm1}$) transitions to neighboring cutting lines[2]—has been measured by photoluminescence excitation spectroscopy.[3,4] Anisotropy in optical-absorption spectra has also been studied[5,6] and used to determine the nematic order parameter, indicating the degree of alignment of SWNTs. Separate parallel and perpendicular π plasmons have also been identified from anisotropic absorption features in the UV region.[6,7]

It has been previously reported[8] that vertically aligned SWNTs (VA-SWNTs) synthesized by the alcohol catalytic chemical-vapor deposition (ACCVD) method[9] exhibit a characteristic Raman peak in the radial breathing mode (RBM) region at approximately 181 cm^{-1} for excitation with 488 nm light. Contrary to expectation, however, the intensity of this peak was found to be strongest for incident light polarized *perpendicular* to the VA-SWNT alignment direction. Other weaker peaks were also found to exhibit the same behavior. Furthermore, these peaks could not be accurately assigned to specific (n,m) chiralities by comparing to calculations of interband transition energies (the so-called Kataura plot). They were thus attributed[8] to a resonance with $E_{\mu,\mu\pm1}$ caused by perpendicularly polarized excitation.[2]

To clarify the origin of this RBM anomaly, in this study we systematically measured resonance Raman spectra for different polarization conditions and quantitatively analyzed the spectra using theoretical models and a more accurate Kataura plot. Our findings indicate the differing polarization dependencies arise *not* from perpendicularly polarized excitation of SWNTs but from the morphology of the VA-SWNT array. We note that although it has been known for some time that excitons are responsible for the optical properties of SWNTs,[10,11] the band-model concept of cutting lines and selection rules for interband transitions—on which the polarized Raman discussion is based—are still valid.

II. EXPERIMENTAL DETAILS

A. Measurement of polarization-dependent Raman spectra

VA-SWNTs were synthesized on a quartz substrate by the ACCVD method, as described in detail elsewhere.[12,13] Based on our previous analysis of this and similar samples by high-resolution transmission electron microscopy, the SWNT fraction of this sample is believed to be more than 99.9%. After VA-SWNT synthesis, the substrate was cleaved to reveal a cross section of the array, which had a height of approximately 15 μm as determined from observation by scanning electron microscopy (SEM). For measurement of resonance Raman spectra, this fractured piece was mounted onto a rotatable stage such that the alignment direction was in the plane of the stage and the linearly polarized excitation laser

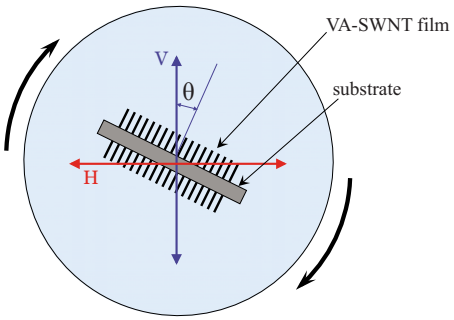

FIG. 1. (Color online) Top view of a rotating stage with mounted VA-SWNT array. Incident light is polarized along *V*, and a polarizer selects the outgoing polarization along either *V* or *H*.

was incident normal to the cross section of the VA-SWNT array.

The two measurement configurations used in these experiments are shown in Fig. 1. Unless otherwise stated, the light source used in all measurements was a 488 nm (2.54 eV) Ar laser with a 0.2 mW spot approximately 2 μm in diameter. The micro-Raman system consisted of an Olympus BX51 optical microscope, a Chromex 500is spectrometer, and an Andor DV401A-BV CCD detector. The incident light was sent through a linear polarizer after passing through a bandpass filter, and the scattered light was filtered using a dichroic mirror. The polarization of the incident light was the same for both configurations but the polarization of the scattered light was selected by changing the orientation of a polarizer placed in the outgoing light path. A scrambler was coupled to the polarizer to prevent polarization-dependent losses in the optical fiber connecting the micro-Raman system and the monochromator. The *VV* configuration indicates that the selected polarization of the scattered light has the same orientation as the incident light (i.e., both vertical). Similarly, the *VH* configuration means the selected polarization of the scattered light is perpendicular to that of the incident light. Once the optics had been fixed, the angle θ between the incident light polarization and the SWNT alignment direction was changed by rotating the sample stage. Measurements were made in 15° increments for values of θ from 0° to 90°.

B. Preparation of stretch-aligned SWNTs

For the purpose of comparison, polarization-dependent resonance Raman spectra of a stretch-aligned SWNT-polymer sample were also obtained using the same Raman system and configurations. The sample was prepared by first mixing 20 mg of purified CoMoCat SWNTs in 10 g of D_2O containing 1 wt % sodium dodecyl benzene sulfonate. This solution was ultrasonicated with a horn-type ultrasonicator (Hielscher Ultrasonics GmbH UP400S with H3/Micro Tip 3) for 30 min at a power flux level of 368 W cm^{-2} (90% rated capacity). Following ultrasonication, the dispersion was ultracentrifuged (Hitachi Koki himac CS120GX with a S100AT6 fixed-angle rotor) for 1 h at 163 000 g and the supernatant collected. Poly-vinyl alcohol (PVA) powder (Wako Pure Chemical Industry, polymerization degree 1500) was dissolved at 15 wt % in 80 °C distilled water for 10 min, then cooled to room temperature. This was then added into the SWNT suspension and thoroughly mixed. The mixture was poured into a Petri dish and allowed to polymerize at room temperature for 24 h. The resulting gray solid was then heated to 80 °C and gently stretched to four or five times its original length.

III. RESULTS AND DISCUSSIONS

A. Polarization-dependent intensity relations

According to Raman selection rules, the RBM (which has *A* symmetry) is allowed only when the incident and scattered photons are either both parallel or both perpendicular to the SWNT axis. Excitation of the RBM by light polarized perpendicular to the SWNT axis is therefore possible,[2] thus we investigate this possibility to test our previous hypothesis.[8] The expected polarization-dependent intensities of allowable excitations were calculated for both *VV* and *VH* configurations (see Appendix for details). For an isolated SWNT in the *VV* configuration, if the scattered light is polarized along the SWNT axis, the observed intensity $I_{VV}^{\parallel\parallel}$ is described by

$$I_{VV}^{\parallel\parallel} \propto I_{\mathrm{in}}|\boldsymbol{E}\cdot\boldsymbol{\mu}_{\parallel}|^2 I_{\mathrm{sc}}|\boldsymbol{\mu}_{\parallel}\cdot\boldsymbol{E}|^2. \quad (1)$$

I_{in} and I_{sc} are the respective intensities of the incident and scattered light, and the electric field vector of the incident photon is represented by $\boldsymbol{E}$. Expressions for the two allowable cases are

$$I_{VV}^{\parallel\parallel} \propto 2\cos^4\theta\langle\cos^4\varphi\rangle + 6\cos^2\theta\sin^2\theta\langle\sin^2\varphi\cos^2\varphi\rangle + \frac{3}{4}\sin^4\theta\langle\sin^4\varphi\rangle, \quad (2)$$

$$I_{VV}^{\perp\perp} \propto (8-28\sin^2\theta+23\sin^4\theta)\langle\sin^4\varphi\rangle + (32\sin^2\theta-40\sin^4\theta)\langle\sin^2\varphi\rangle + 8\sin^4\theta, \quad (3)$$

where the symbols $\parallel$ and $\perp$ indicate the incident and scattered polarization orientations with respect to the SWNT axis. The degree of alignment within the sample can be expressed by the *nematic order parameter*, $S=\frac{1}{2}(3\langle\cos^2\varphi\rangle-1)$, which can be found from experimentally obtained orientation-dependent intensity measurements[6,14] (see Appendix). The value $S\approx 0.75$ has been determined for our VA-SWNTs based on both polarization-dependent optical absorption[6] and x-ray absorption spectra[15] (perfect alignment corresponds to a value $S=1$.) In the following discussion, experimentally obtained data are compared to these intensity relations to test the hypothesis of perpendicularly polarized RBM excitation.

B. Aligned SWNTs in PVA

We first look at the stretch-aligned CoMoCat-PVA sample. If all the SWNTs are well aligned, the optical excitations are expected to exhibit the so-called "antenna effect," where excitations are strongest for polarization along the SWNT axis and weakest for perpendicular excitation. This is clearly illustrated by the absorption spectra shown in Fig.

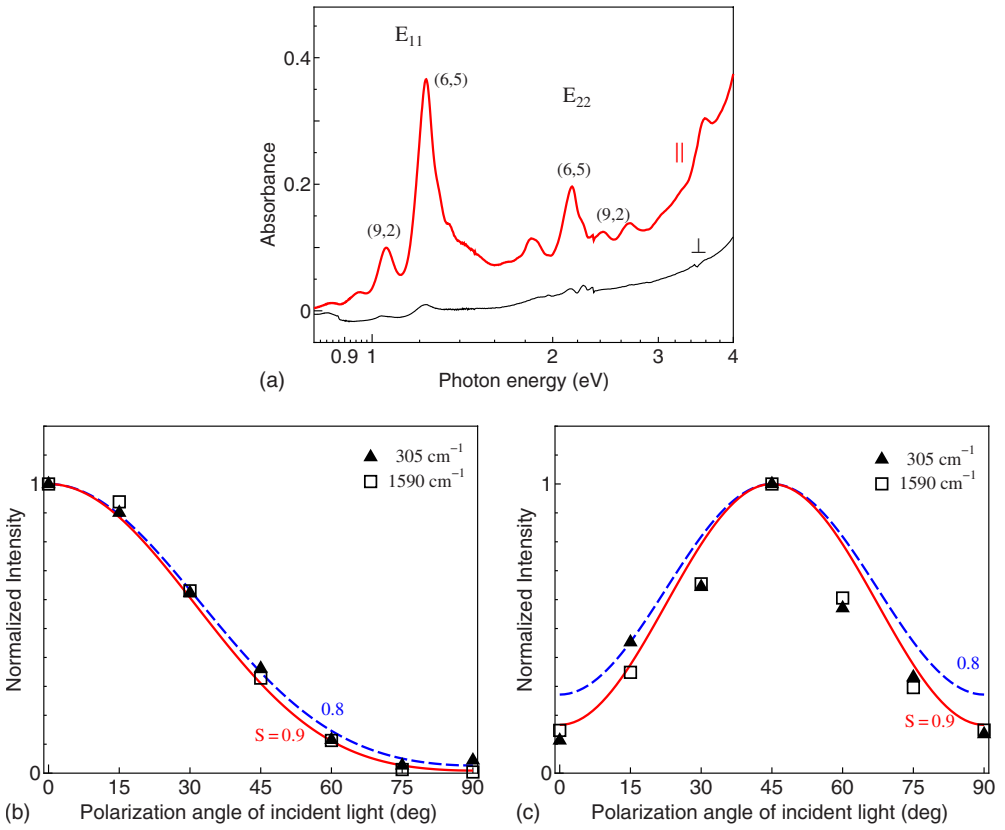

FIG. 2. (Color online) (a) Optical-absorption spectra from a stretched CoMoCat-PVA array. Incident light is polarized parallel (∥) and perpendicular (⊥) to the stretching direction. Lower panels show normalized RBM peak intensities as a function of incident light polarization angle for (b) *VV* and (c) *VH* configurations. Solid and dashed lines are intensity calculations for parallel excitation assuming different order parameters (see Appendix).

2(a). The upper (lower) spectrum was obtained with the incident light polarized parallel (perpendicular) to the stretching direction of the CoMoCat-PVA sample, which is believed to be the SWNT alignment direction. The clear polarization anisotropy in optical absorption illustrates the antenna effect, and comparing the (6,5) absorption peak intensities yields an order parameter[6,14] $S \approx 0.99$, indicating excellent alignment of CoMoCat SWNTs within the stretched polymer matrix.

After confirming the excellent alignment, polarization-dependent resonant Raman spectra were measured as described in Sec. II. The two dominant Raman features were the G band at 1590 cm^{-1} and an RBM peak at 305 cm^{-1} (full spectra can be found in the Appendix). Normalized intensities for these two peaks for both *VV* and *VH* configurations are plotted in Figs. 2(b) and 2(c), respectively. The fitting curves show our calculated angular-dependent intensities for nematic order parameters $S=0.8$ (dashed lines) and $S=0.9$ (solid lines). The solid lines match the data very well, again indicating excellent alignment of the SWNTs within the stretch-aligned sample and validating our intensity calculations.

C. Vertically aligned SWNT array

Next we examine the VA-SWNT array. Figure 3 shows a series of resonance Raman spectra obtained for both *VV* and *VH* configurations from an as-grown VA-SWNT array. Considering that the position of the laser spot may shift during rotation, values plotted are averages of three independent measurements. In Fig. 3(a), different peaks appear to have opposite polarization dependencies: the 160 and 203 cm^{-1} peaks (hereafter referred to as the {203 cm^{-1}} group) have decreasing intensity with increasing polarization angle θ whereas the 145, 181, 244, and 256 cm^{-1} peaks (hereafter referred to as the {181 cm^{-1}} group) *increase* in intensity as θ approaches 90°. The {203 cm^{-1}} group exhibits expected behavior (i.e., that of the SWNT-PVA sample) while the {181 cm^{-1}} group peaks are those which have anomalous polarization dependence.[8]

Careful inspection of Fig. 3(c) reveals a slight upshift of the G band when the incident polarization angle increases from 0° to 90°. This is attributed to heating of the SWNTs because of stronger absorption of the laser when $\theta=0$ (i.e., polarization along the SWNT axis), which is known to reduce both the energy and intensity of the Raman peaks.[16] After normalizing and correcting for heating-induced intensity effects (see Appendix), we obtained the angle dependence of the various RBM peaks, as shown in Fig. 4. The solid (dashed) line shows the expected polarization-dependent intensity for parallel (perpendicular) excitation for the order parameter=0.75. It is clear that the {203 cm^{-1}} group behaves as expected for parallel excitation, however the peak intensities of the {181 cm^{-1}} group are essentially independent of polarization angle, deviating significantly

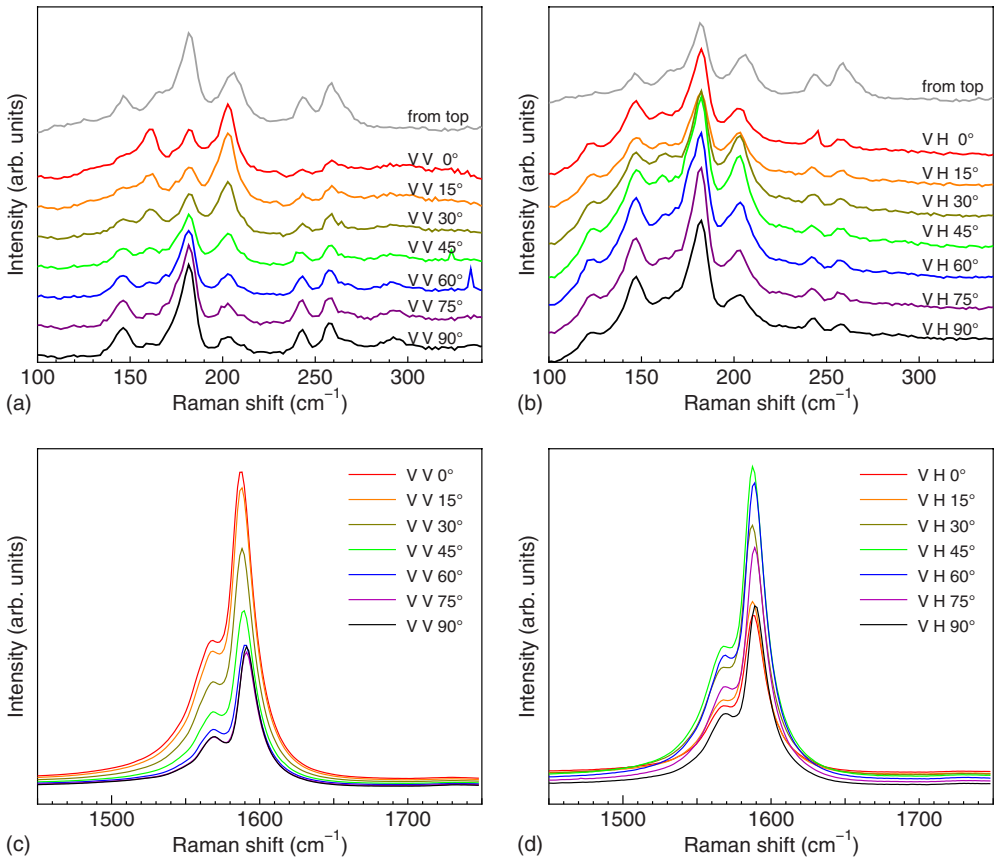

FIG. 3. (Color online) Polarization angle dependence of the RBM [(a) and (b)] and G band [(c) and (d)] of a VA-SWNT array for 488 nm laser excitation. The incident polarization angle was changed from 0° (along the alignment direction) to 90° (perpendicular to the alignment direction) in 15° steps. Left and right panels correspond to *VV* and *VH* configurations, respectively.

from expectation for perpendicularly polarized excitation. Similar disagreement from expectation for perpendicularly polarized excitation is seen in the *VH* case as well (see Appendix).

This clear disagreement with expected intensity relations casts serious doubt on the perpendicularly polarized excitation hypothesis so we investigated the VA-SWNT array in more detail to look for an alternative explanation. A high-resolution SEM image of the SWNT array cross section is shown on the left side of Fig. 5 (low magnification in inset). Among the vertically aligned bundles, "stray" SWNTs can be seen dispersed throughout the array. These stray SWNTs have little preferred orientation and appear to be nearly isolated. This morphology is illustrated in the right panel of Fig. 5.

One finding that provides a clue as to the role of these stray SWNTs is that the {181 cm^{-1}} group peaks disappear if the alignment of the SWNTs is disturbed, e.g., by dispersion in D_2O and drying [Fig. 6(a)]. After dispersion, these peaks cannot be recovered by any process such as heating, etc.,

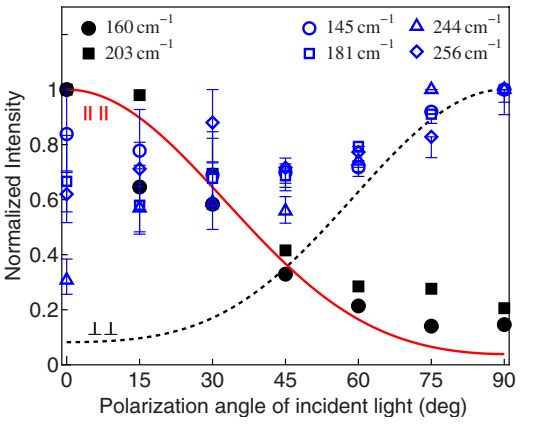

FIG. 4. (Color online) Polarization dependence of RBM peak intensities (*VV* configuration). Error bars indicate uncertainty after correcting for temperature effects (see text and Appendix). Solid (dashed) lines are calculated intensities expected for parallel (perpendicular) excitation.

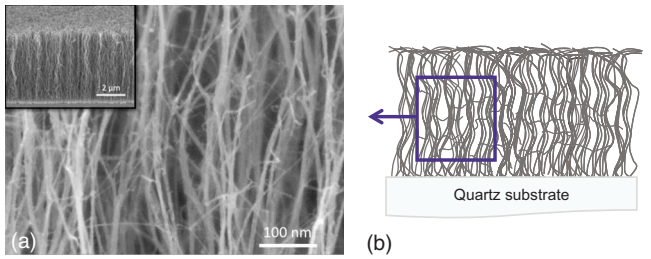

FIG. 5. (Color online) Left: high-resolution SEM image of the cross section of a VA-SWNT array (inset: low magnification). Right: illustration of the array morphology, with isolated SWNTs dispersed among the aligned bundles.

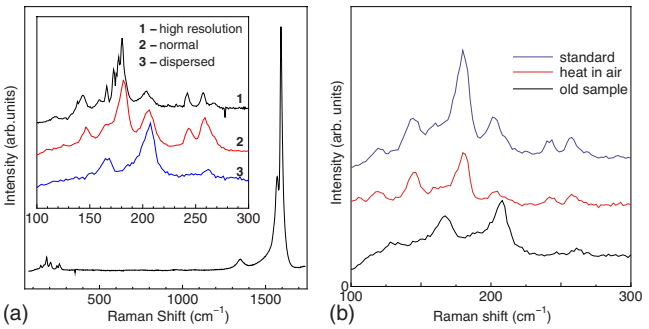

FIG. 6. (Color online) (a) Raman spectra taken from the top of a VA-SWNT array. Inset shows the RBM region with high-resolution (topmost) and with normal resolution before (middle) and after (lower) dispersion in D_2O. (b) RBM spectra taken from the top of a VA-SWNT array after synthesis (top), after storage for 2 years (bottom), and after heating at 300 °C (middle). All spectra in (b) are from the same VA-SWNT array.

although the {203 cm^{-1}} group peaks remain. This indicates that the {181 cm^{-1}} group is somehow morphology dependent, and significantly decreases in intensity when bundled with other SWNTs. Further evidence for isolated SWNTs within the array was obtained from high-resolution Raman spectra. The spectra shown in Fig. 6(a) are from the same VA-SWNT array but were obtained by changing the spectrometer grating in the Raman system described in Sec. II from 1200 to 2400 gratings/mm. Spectrum No. 1 in the inset reveals that the strong 181 cm^{-1} peak is actually composed of three sharp peaks. Unlike optical absorption, the resonance Raman signal from suspended, isolated SWNTs is known to be very strong,[17,18] thus it is reasonable to obtain such a strong signal despite the array containing just a small fraction of isolated SWNTs.

It has also been found that the intensities of these peaks slowly decrease[8] until essentially disappearing after storage in air for a long period of time (i.e., months or years). However, these peaks can be recovered by heating the sample at 300 °C for 10 min, as shown in Fig. 6(b). This suggests adsorption of molecules onto the SWNTs (primarily H_2O) is responsible for the change in peak intensity. Such environment sensitivity can be expected for isolated or nearly isolated SWNTs.

These results indicate a morphology dependence of the Raman spectra. Thus, we attempted to assign all the RBM peaks using a Kataura plot showing E_{ii} transitions (from the ith cutting line in the valence band to the ith cutting line in the conduction band) while taking into account both bundled and isolated SWNTs. We used the relationship between SWNT diameter and RBM frequency $\omega_{\mathrm{RBM}}=\frac{217.8}{d_t}+15.7$ cm^{-1} (d_t is the SWNT diameter in nanometers), which had been determined from fitting of experimentally obtained data[19] from VA-SWNTs synthesized by the same method as used in this study, thus should be most accurate. The area of interest is shown in Fig. 7. Here we plot the RBM peaks found in polarization-dependent resonance Raman spectra obtained with 488, 514, and 633 nm excitation lasers (spectra for 633 nm excitation were obtained using the same method as described in Sec. II and the 514 nm data are

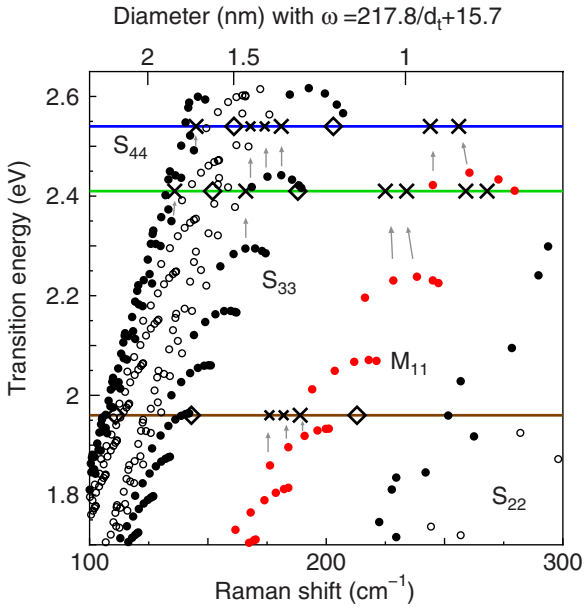

FIG. 7. (Color online) Kataura plot showing E_{ii} transition energies. SWNT diameter and Raman shift are related by the equation $\omega_{\mathrm{RBM}}=\frac{217.8}{d_t}+15.7$ (cm^{-1}). Metallic $[(2n+m)\mathrm{mod}\ 3=0]$ and semiconducting $[(2n+m)\mathrm{mod}\ 3\neq 0]$ branches are labeled in the figure, with type-I and type-II semiconducting SWNTs indicated by open and filled circles, respectively. Horizontal lines at 2.54, 2.41, and 1.96 eV indicate the respective excitation energies of the 488, 514, and 633 nm lasers used to obtain resonance Raman spectra. Diamonds denote peaks behaving as parallel excitation, while crosses denote those behaving oppositely.

from Ref. 8). Peaks exhibiting the antenna effect are indicated by a diamond and those which do not are indicated by a cross.

The key to interpret our results is that this Kataura plot is based on experimentally obtained data,[19] i.e., primarily SWNT bundles. The transition energy for an isolated SWNT

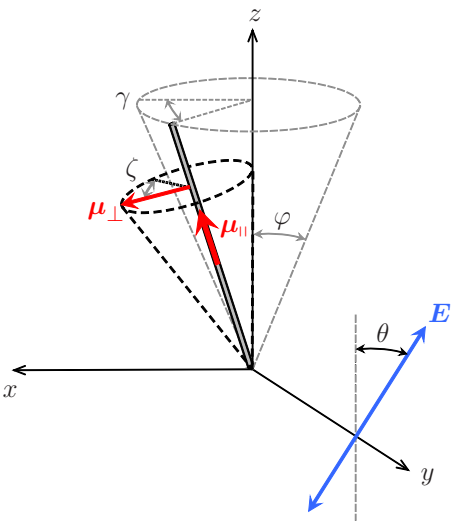

FIG. 8. (Color online) Excitation geometry and orientation of parallel and perpendicular dipoles ($\boldsymbol{\mu}$) for VA-SWNTs with some distribution around the substrate normal (z axis).

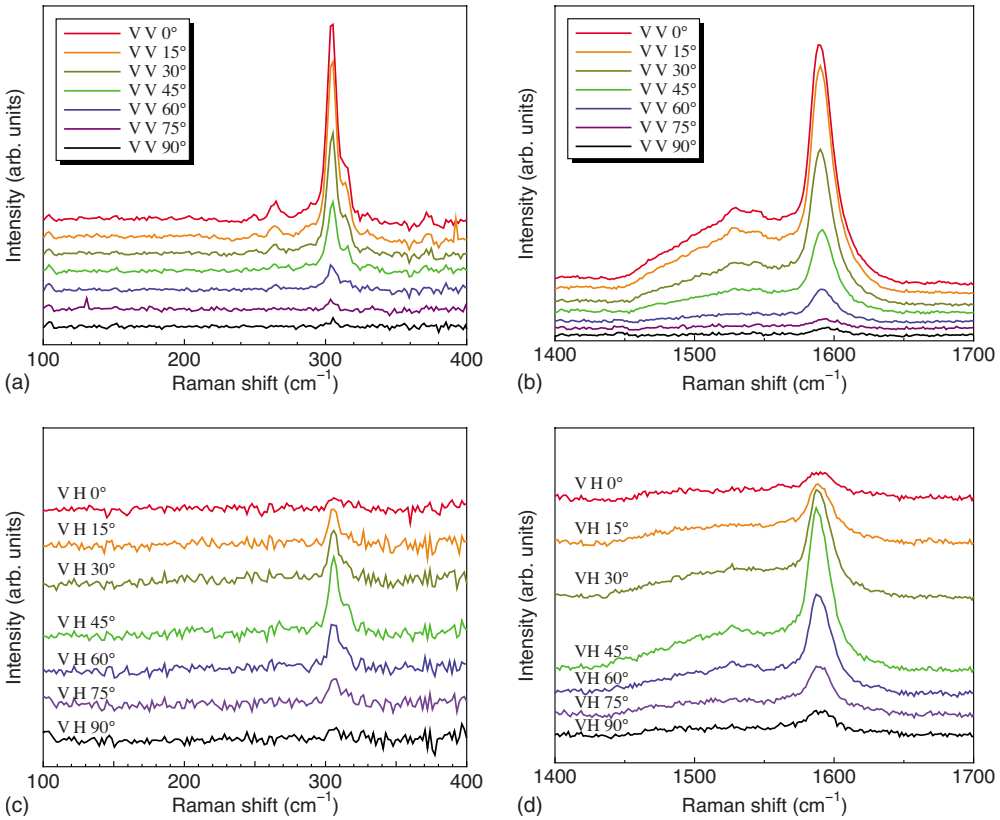

FIG. 9. (Color online) RBM (left) and G band (right) Raman spectra of CoMoCat-PVA arrays with the incident polarization changing from 0° (along stretching direction) to 90° (perpendicular to the stretching direction). Spectra are shown for both *VV* (upper panels) and *VH* orientations (lower panels).

is known to be relatively blueshifted with respect to the bundle transition energy, and bundling broadens the resonance window by as much as 120 meV.[20] Therefore, when the excitation laser is polarized perpendicular to the SWNT alignment direction, we excite primarily isolated SWNTs. The transition energies of these SWNTs are shifted upward relative to the bundle transition energy and become visible in the spectra. The same SWNTs, when in bundles, will be slightly downshifted, thus less resonant with the excitation laser. Taking into account the bundle-induced broadening of the resonance window and referring to the resonance Raman-scattering map in Ref. 19, nearly every peak can be assigned to E_{ii} transitions, as shown in Fig. 7. We note that {203 cm^{-1}} group peaks (diamonds) correspond to SWNTs with E_{ii} energies close to the laser excitation energy, which are bundled tubes within the array. Conversely, the {181 cm^{-1}} group peaks correspond to isolated SWNTs whose E_{ii} energies lie slightly below the excitation laser energy. When isolated, the upshift of the excitation window, indicated by the gray arrows, brings the point closer to the laser energy, causing the RBM intensity to increase. This occurs primarily when the laser is polarized perpendicular to the general alignment direction of SWNTs within the array. Furthermore, the group of peaks near 181 cm^{-1} seen in Fig. 6(a) nicely matches the family of peaks slightly below the 488 nm excitation energy. Bundle-induced broadening of the RBM peaks would make these difficult to distinguish if they were not isolated but when isolated, each peak becomes apparent. We therefore conclude that the morphology of the SWNT array is responsible for the apparently anomalous polarization dependence seen in some RBM peaks, and perpendicular polarization with respect to the alignment direction causes parallel excitation of isolated SWNTs within the array.

IV. CONCLUSION

In this paper, we investigate the polarization dependence of RBM peaks in resonance Raman spectra of vertically aligned SWNTs. Excitation by perpendicularly polarized light has been suggested to explain previous results but here we show this explanation is unlikely. In addition to significant deviation from theoretical calculations of polarization-dependent intensity, the presence of isolated SWNTs is evidenced by high-resolution Raman spectra. SEM observation also reveals many isolated SWNTs distributed among the array. By taking into account the broadening and shift of the resonance window due to SWNT bundling, nearly all RBM peaks could be identified using an experimentally obtained Kataura plot. After revisiting this issue, we conclude that the anomalous polarization dependence exhibited by some RBM peaks is due to the mixture of aligned bundles and randomly oriented isolated SWNTs dispersed throughout the vertically aligned array.

ACKNOWLEDGMENTS

Part of this work was financially supported by Grants-in-

Aid for Scientific Research (Grants No. 19206024 and No. 19054003) from the Japan Society for the Promotion of Science, SCOPE (Grant No. 051403009) from the Ministry of Internal Affairs and Communications, NEDO (Japan), and by the Global COE Program "Global Center for Excellence for Mechanical Systems Innovation," MEXT, Japan.

APPENDIX

1. Multiple-dipole approximation

a. Scattering geometry

The dipole approximation allows for optical transitions between subbands of the valence and conduction bands $E^v_\mu \rightarrow E^c_{\mu'}$, where $\mu' = \mu$ for light polarized along the nanotube axis[1,21] and $\mu' = \mu \pm 1$ for light polarized perpendicular to the nanotube axis.[2] Thus, by changing the light polarization relative to the SWNT, it is possible to select different symmetry-allowed phonon modes.[22]

In the following discussion, we use the scattering geometry shown in Fig. 8, which is based on that in Ref. 14. This establishes the z axis as the SWNT alignment direction (i.e., normal to the substrate surface), and assumes that the VA-SWNTs are straight and distributed uniformly about this axis. The orientation of a given SWNT is defined by two angles φ $(0 \leq \varphi \leq \frac{\pi}{2})$, which is the angle between SWNT axis and z axis, and γ $(0 \leq \gamma \leq 2\pi)$, which is the rotational angle of a plane constructed by the SWNT axis and the z axis. Selection rules allow two dipoles to contribute to the first-order Raman-scattering process. These dipoles are oriented parallel ($\boldsymbol{\mu}_\parallel$) and perpendicular ($\boldsymbol{\mu}_\perp$) to the nanotube axis.

b. Approximation of the Raman process

The Raman-scattering process can be approximated as absorption and emission of photons with unequal energies, where the emission process is simply time-reversed absorption. Here we use this approximation, taking into account contributions from both parallel and perpendicular dipoles.

As described in Sec. II, we adopt two configurations, *VV* and *VH*, to measure spectra for different scattering geometries. According to the selection rules, the RBM (A mode) can only be excited when incident and scattered photons are both parallel or both perpendicular to the nanotube axis. Thus, we discuss these two cases below, using the notation "$\parallel\parallel$" and "$\perp\perp$."

We first consider the case of only one SWNT in the *VV* configuration. If the scattered light is polarized along the SWNT axis, the observed intensity $I^{\parallel\parallel}_{VV}$ is described by

$$I^{\parallel\parallel}_{VV} \propto I_{\mathrm{in}} |\boldsymbol{E} \cdot \boldsymbol{\mu}_\parallel|^2 I_{\mathrm{sc}} |\boldsymbol{\mu}_\parallel \cdot \boldsymbol{E}|^2, \tag{A1}$$

where I_{in} and I_{sc} are the respective intensities of the incident and scattered light, and the electric field vector $\boldsymbol{E}$ of the incident photon, expressed by $\boldsymbol{E}=(-\sin\theta, 0, \cos\theta)$, only has components in the x-z plane. Taking into account the distribution of the SWNTs, we obtain the full expression for the intensity of the scattered signal,

$$\begin{aligned} I^{\parallel\parallel}_{VV} &\propto \int_0^{\pi/2}\int_0^{2\pi} I_{\mathrm{in}} |\boldsymbol{E} \cdot \boldsymbol{\mu}_\parallel|^2 I_{\mathrm{sc}} |\boldsymbol{\mu}_\parallel \cdot \boldsymbol{E}|^2 \rho(\varphi) d\gamma d\varphi \\ &\propto \int_0^{\pi/2}\int_0^{2\pi} (-\sin\theta \sin\varphi \cos\gamma \\ &\quad + \cos\theta \cos\varphi)^4 \rho(\varphi) d\gamma d\varphi \\ &\propto \int_0^{\pi/2}\int_0^{2\pi} (\sin^4\theta \sin^4\varphi \cos^4\gamma + \cos^4\theta \cos^4\varphi \\ &\quad + 6 \sin^2\theta \cos^2\theta \sin^2\varphi \cos^2\varphi \cos^2\gamma \\ &\quad - 4 \sin\theta \cos^3\theta \sin\varphi \cos^3\varphi \cos\gamma \\ &\quad - 4 \sin^3\theta \cos\theta \sin^3\varphi \cos\varphi \cos^3\gamma) \rho(\varphi) d\gamma d\varphi, \end{aligned} \tag{A2}$$

which simplifies to

$$\begin{aligned} I^{\parallel\parallel}_{VV} &\propto 2\cos^4\theta \langle \cos^4\varphi \rangle + 6 \cos^2\theta \sin^2\theta \langle \sin^2\varphi \cos^2\varphi \rangle \\ &\quad + \frac{3}{4} \sin^4\theta \langle \sin^4\varphi \rangle. \end{aligned} \tag{A3}$$

Similarly, the $I^{\perp\perp}_{VV}$ case becomes

$$\begin{aligned} I^{\perp\perp}_{VV} &\propto \int_0^{\pi/2}\int_0^{2\pi}\int_0^{2\pi} I_{\mathrm{in}} |\boldsymbol{E} \cdot \boldsymbol{\mu}_\perp|^2 I_{\mathrm{sc}} |\boldsymbol{E} \cdot \boldsymbol{\mu}_\perp|^2 \rho(\varphi) d\zeta d\gamma d\varphi \\ &\propto (8 - 28 \sin^2\theta + 23 \sin^4\theta) \langle \sin^4\varphi \rangle \\ &\quad + (32 \sin^2\theta - 40 \sin^4\theta) \langle \sin^2\varphi \rangle + 8 \sin^4\theta. \end{aligned} \tag{A4}$$

We use a similar approach to obtain the polarization dependence for the two *VH* cases,

$$\begin{aligned} I^{\parallel\parallel}_{VH} &\propto \int_0^{\pi/2}\int_0^{2\pi} I_{\mathrm{in}} |\boldsymbol{E} \cdot \boldsymbol{\mu}_\parallel|^2 I_{\mathrm{sc}} |\boldsymbol{f} \cdot \boldsymbol{\mu}_\parallel|^2 \rho(\varphi) d\gamma d\varphi \\ &\propto \frac{3}{4} \sin^2\theta \cos^2\theta \langle \sin^4\varphi \rangle + 2 \cos^2\theta \sin^2\theta \langle \cos^4\varphi \rangle \\ &\quad + (\sin^4\theta + \cos^4\theta - 4 \sin^2\theta \cos^2\theta) \langle \sin^2\varphi \cos^2\varphi \rangle, \end{aligned} \tag{A5}$$

where $\boldsymbol{f}=(-\cos\theta, 0, -\sin\theta)$ denotes the orientation of a polarizer for observing the scattered light, and is perpendicular to the incident light polarization,

$$\begin{aligned} I^{\perp\perp}_{VH} &\propto \int_0^{\pi/2}\int_0^{2\pi}\int_0^{2\pi} I_{\mathrm{in}} |\boldsymbol{E} \cdot \boldsymbol{\mu}_\perp|^2 I_{\mathrm{sc}} |\boldsymbol{f} \cdot \boldsymbol{\mu}_\perp|^2 \rho(\varphi) d\zeta d\gamma d\varphi \\ &\propto 4 - 6 \sin^2\theta \cos^2\theta + 3(27 \sin^2\theta \cos^2\theta - 4) \langle \cos^4\varphi \rangle \\ &\quad + 2(4 - 21 \sin^2\theta \cos^2\theta) \langle \cos^2\varphi \rangle. \end{aligned} \tag{A6}$$

As shown in Refs. 6 and 14, the anisotropy can be determined from optical absorption for orthogonal polarizations. The absorption cross sections of SWNTs both parallel and perpendicular to the nanotube axis are noted as $\Lambda_\parallel$ and $\Lambda_\perp$. Experimentally, the absorption of incident light parallel $[I_{exp}(\theta=0)]$ and perpendicular $[I_{exp}(\theta=\frac{\pi}{2})]$ to the alignment direction are measured to obtain the anisotropy using the following equation:

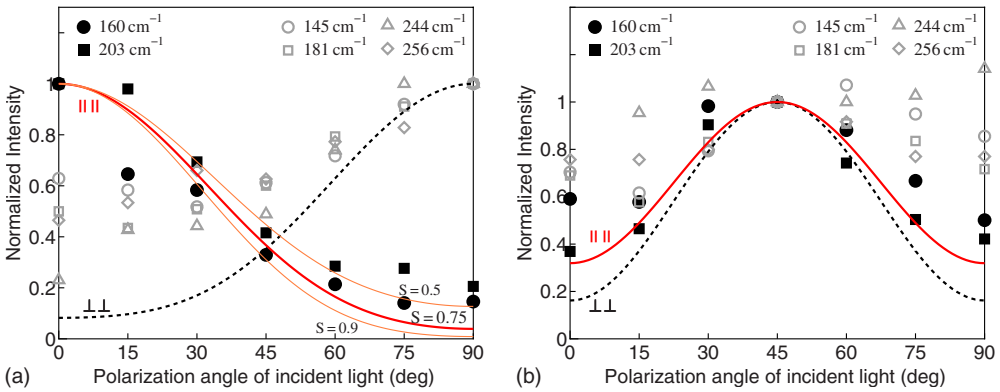

FIG. 10. (Color online) RBM peak intensities for incident light polarization angles from 0° to 90° with respect to the VA-SWNT alignment direction. Both *VV* (left) and *VH* (right) configurations are shown. Curves show theoretical angle-dependent intensity profiles for parallel and perpendicular excitations.

$$\frac{I_{exp}(0) - I_{exp}\left(\frac{\pi}{2}\right)}{I_{exp}(0) + 2I_{exp}\left(\frac{\pi}{2}\right)} = \frac{\Lambda_{\parallel} - \Lambda_{\perp}}{\Lambda_{\parallel} + 2\Lambda_{\perp}}\left(\frac{3\langle\cos^2\varphi\rangle - 1}{2}\right)$$

$$= \frac{\Lambda_{\parallel} - \Lambda_{\perp}}{\Lambda_{\parallel} + 2\Lambda_{\perp}} S. \tag{A7}$$

$S = \frac{1}{2}(3\langle\cos^2\varphi\rangle - 1)$ is the *nematic order parameter*, which indicates the degree of alignment of the sample. If the absorption cross sections $\Lambda_{\parallel}$ and $\Lambda_{\perp}$ are known, the order parameter S and distribution $\rho(\varphi)$ can be obtained and applied to our polarization-dependent Raman-scattering studies.

2. Polarized Raman spectra of stretch-aligned SWNTs in PVA

The polarization-dependent Raman spectra of stretch-aligned SWNTs in PVA are shown in Fig. 9.

3. RBM peak dependence of polarization angle

RBM peak intensities for incident light polarization angles from 0° to 90° with respect to the VA-SWNT alignment direction are shown in Fig. 10.

4. Laser heating effects

When measuring Raman spectra, the SWNT sample can be heated considerably by the incident laser. It has been found that all six components of the G band decrease in energy with increasing temperature.[16] The position of the G$^+$ peak is described by the function,[16]

$$\omega(T) = \omega_0 - \frac{A}{\exp(B\hbar\omega_0/k_B T) - 1}, \tag{A8}$$

where $\hbar$ is Planck's constant, k_B is Boltzmann's constant, T is the sample temperature, $\omega_0 = 1594$ cm^{-1}, $A = 38.4$ cm^{-1}, and $B = 0.438$. Therefore, the sample temperature can be inferred directly from the G$^+$ peak position. Since increasing laser power not only increases the sample temperature but also increases the Raman intensity,[16] it is also necessary to remove this effect to obtain the real intensity dependence on polarization angle.

In the polarization-dependent measurements presented here, the G band peaks were found to slightly increase in frequency when the incident polarization angle changed from 0° to 90°. This is because SWNTs more strongly absorb light that is polarized along the tube axis, which causes heating of the SWNT array. For the *VV* configuration, the G$^+$ peak changed from 1587.5 to 1591.5 cm^{-1}. Using Eq. (A8), the sample temperature is found to be approximately 500 K at 0° and 360 K at 90°. The G$^+$ peak frequency shows a similar trend for the *VH* configuration. After correcting for this heating effect (not shown), the G$^+$ peak intensities are in better agreement with the intensity calculations for both *VV* and *VH* configurations.

To determine the effect of heating on RBM intensities, we measured Raman spectra with various laser powers and determined the temperature from the G$^+$ peak position. We then normalized the spectra after correcting for the temperature-induced decrease in G$^+$ intensity. Noting that G$^+$ and RBM peaks are similarly affected by laser power, this effect can be corrected for by normalizing with the temperature-corrected G$^+$ peak intensity. The temperature dependence on peak intensity for the four main RBM peaks is shown in Fig. 11.

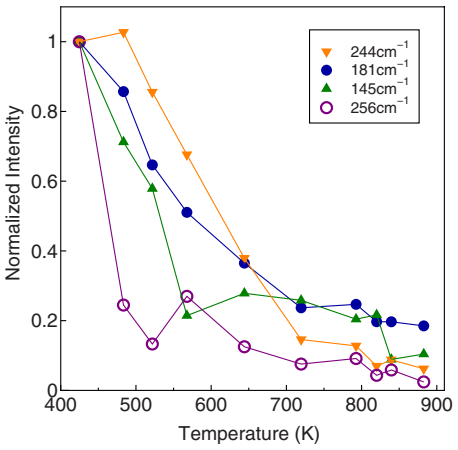

FIG. 11. (Color online) Temperature dependence of RBM peak intensities for VA-SWNTs.

The {181 cm^{-1}} group peaks decrease almost linearly by about 80% until 720 K, then become constant at higher temperatures. Chiashi *et al.*[16] similarly reported two different temperature-dependent intensity trends for high-pressure carbon monoxide (HiPco) SWNTs but in their case, some peak intensities were also found to increase. Regardless of this difference, we can use the trends seen in Fig. 11 to obtain the correct polarization-dependent intensity relationship (the corrected form of Fig. 10). This is shown for the *VV* configuration used to obtain the data plotted in Fig. 4.

*maruyama@photon.t.u-tokyo.ac.jp

[1] R. Saito, G. Dresselhaus, and M. S. Dresselhaus, *Physical Properties of Carbon Nanotubes* (Imperial College Press, London, 1998).
[2] A. Grüneis, R. Saito, J. Jiang, Ge. G. Samsonidze, M. A. Pimenta, A. Jorio, A. G. Souza Filho, G. Dresselhaus, and M. S. Dresselhaus, Chem. Phys. Lett. **387**, 301 (2004).
[3] Y. Miyauchi, M. Oba, and S. Maruyama, Phys. Rev. B **74**, 205440 (2006).
[4] J. Lefebvre and P. Finnie, Phys. Rev. Lett. **98**, 167406 (2007).
[5] M. F. Islam, D. E. Milkie, C. L. Kane, A. G. Yodh, and J. M. Kikkawa, Phys. Rev. Lett. **93**, 037404 (2004).
[6] Y. Murakami, E. Einarsson, T. Edamura, and S. Maruyama, Phys. Rev. Lett. **94**, 087402 (2005).
[7] C. Kramberger, R. Hambach, C. Giorgetti, M. H. Rümmeli, M. Knupfer, J. Fink, B. Büchner, L. Reining, E. Einarsson, S. Maruyama, F. Sottile, K. Hannewald, V. Olevano, A. G. Marinopoulos, and T. Pichler, Phys. Rev. Lett. **100**, 196803 (2008).
[8] Y. Murakami, S. Chiashi, E. Einarsson, and S. Maruyama, Phys. Rev. B **71**, 085403 (2005).
[9] S. Maruyama, R. Kojima, Y. Miyauchi, S. Chiashi, and M. Kohno, Chem. Phys. Lett. **360**, 229 (2002).
[10] F. Wang, G. Dukovic, L. E. Brus, and T. F. Heinz, Science **308**, 838 (2005).
[11] *Carbon Nanotubes: Advanced Topics in the Synthesis, Structure, Properties and Applications*, edited by A. Jorio, M. S. Dresselhaus, and G. Dresselhaus (Springer, New York, 2008).
[12] Y. Murakami, S. Chiashi, Y. Miyauchi, M. Hu, M. Ogura, T. Okubo, and S. Maruyama, Chem. Phys. Lett. **385**, 298 (2004).
[13] S. Maruyama, E. Einarsson, Y. Murakami, and T. Edamura, Chem. Phys. Lett. **403**, 320 (2005).
[14] Y. Murakami, E. Einarsson, T. Edamura, and S. Maruyama, Carbon **43**, 2664 (2005).
[15] C. Kramberger, H. Shiozawa, H. Rauf, A. Grüneis, M. H. Rümmeli, T. Pichler, B. Büchner, D. Batchelor, E. Einarsson, and S. Maruyama, Phys. Status Solidi B **244**, 3978 (2007).
[16] S. Chiashi, Y. Murakami, Y. Miyauchi, and S. Maruyama, Jpn. J. Appl. Phys. **47**, 2010 (2008).
[17] M. Paillet, S. Langlois, L. Marty, A. Iaia, C. Naud, V. Bouchiat, A. M. Bonnot, and J.-L. Sauvajol, J. Phys. Chem. B **110**, 164 (2006).
[18] H. Kataura, T. Ueno, Y. Miyata, K. Yanagi, S. Okubo, S. Suzuki, and Y. Achiba, Proceedings of the 20th International Conference on Raman Spectroscopy, 2006 (unpublished).
[19] P. T. Araujo, S. K. Doorn, S. Kilina, S. Tretiak, E. Einarsson, S. Maruyama, H. Chacham, M. A. Pimenta, and A. Jorio, Phys. Rev. Lett. **98**, 067401 (2007).
[20] C. Fantini, A. Jorio, M. Souza, M. S. Strano, M. S. Dresselhaus, and M. A. Pimenta, Phys. Rev. Lett. **93**, 147406 (2004).
[21] A. Jorio, G. Dresselhaus, M. S. Dresselhaus, M. Souza, M. S. S. Dantas, M. A. Pimenta, A. M. Rao, R. Saito, C. Liu, and H. M. Cheng, Phys. Rev. Lett. **85**, 2617 (2000).
[22] M. S. Dresselhaus, G. Dresselhaus, R. Saito, and A. Jorio, Phys. Rep. **409**, 47 (2005).